Regional identification of information flow termination of electrohysterographic signals: Towards understanding human uterine electrical propagation

Xu, Y., Hao, D., Taggart, M. J. & Zheng, D

DOI 10.1016/j.cmpb.2022.106967
ISSN 0169-2607

Publisher: Elsevier

Computer Methods and Programs in Biomedicine 223 (2022) 106967

Contents lists available at ScienceDirect

Computer Methods and Programs in Biomedicine

journal homepage: www.elsevier.com/locate/cmpb

Regional identification of information flow termination of electrohysterographic signals: Towards understanding human uterine electrical propagation

Yuhang Xu[a,*], Dongmei Hao[b], Michael J. Taggart[c], Dingchang Zheng[a,*]

[a] Research Center for Intelligent Healthcare, Institute of Health and Wellbeing, Coventry University, Priory Street, Coventry, CV1 5FB, UK
[b] College of Life Science and Bioengineering, Beijing University of Technology, Beijing, 100124, China
[c] Biosciences Institute, Newcastle University, International Center for Life, Newcastle upon Tyne, NE1 4EP, UK

ARTICLE INFO

Article history:
Received 2 July 2021
Revised 13 June 2022
Accepted 17 June 2022

Keywords:
Electrohysterogram (EHG)
Uterine contraction
Directed information
Human uterine electrical propagation

ABSTRACT

Background and Objective: The uterine electrohysterogram (EHG) contains important information about electrical signal propagation which may be useful to monitor and predict the progress of pregnancy towards parturition. Directed information processing has the potential to be of use in studying EHG recordings. However, so far, there is no directed information-based estimation scheme that has been applied to investigating the propagation of human EHG recordings. To realize this, the approach of directed information and its reliability and adaptability should be scientifically studied.

Methods: We demonstrated an estimation scheme of directed information to identify the spatiotemporal relationship between the recording channels of EHG signal and assess the algorithm reliability initially using simulated data. Further, a regional identification of information flow termination (RIIFT) approach was developed and applied for the first time to extant multichannel EHG signals to reveal the terminal zone of propagation of the electrical activity associated with uterine contraction. RIIFT operates by estimating the pairwise directed information between neighboring EHG channels and identifying the location where there is the strongest inward flow of information. The method was then applied to publicly-available experimental data obtained from pregnant women with the use of electrodes arranged in a $4-by-4$ grid.

Results: Our results are consistent with the suggestions from the previous studies with the added identification of preferential sites of excitation termination - within the estimated area, the direction of surface action potential propagation towards the medial axis of uterus during contraction was discovered for 72.15% of the total cases, demonstrating that our RIIFT method is a potential tool to investigate EHG propagation for advancing our understanding human uterine excitability.

Conclusions: We developed a new approach and applied it to multichannel human EHG recordings to investigate the electrical signal propagation involved in uterine contraction. This provides an important platform for future studies to fill knowledge gaps in the spatiotemporal patterns of electrical excitation of the human uterus.

1. Introduction

The contractile activity of the uterus is involved in physiological processes such as menstrual cycle, gestation and childbirth. Abnormal uterine contractions (UCs) may lead to severe obstetric complications. For example, inappropriately early activation of the uterus can result in preterm birth which increases the risks of neonatal mortality (accounting for more than 50% of all neona-

* Corresponding authors.
E-mail addresses: yuhang.xu@coventry.ac.uk (Y. Xu), dingchang.zheng@coventry.ac.uk (D. Zheng).

https://doi.org/10.1016/j.cmpb.2022.106967

tal deaths) and numerous health risks for surviving neonates [1,2]. Insufficient uterine activation at term is also a marked pregnancy complication and can result in post-date gestation and postpartum hemorrhage [3,4].

Uterine contraction (UC) is determined by episodic spontaneous electrical action potentials (APs) traveling across the muscle cells of the wall of the uterus. A possible way to distinguish between normal and abnormal activation, and thereby inform clinical diagnosis and intervention for problematic situations, is to investigate the difference between the features of propagation of their underlying electrical stimulation [5]. The information of surface AP propagation revealed by the technique of multi-lead electrohysterogram (EHG), which records uterine electrical activity externally at several points on the abdomen, has demonstrated a potential in this regard and distinguishing the productive UCs from the unproductive UCs [6–11].

The estimation of EHG propagation may be feasible with the use of delay estimators that calculate the timings between EHG signals recorded from different electrodes of a grid. This can, with the acknowledgment of several assumptions, calculate the speed as well as the direction of EHG propagation between electrodes [5,8,10,12–16]. The Maximum Likelihood (ML) method for delay estimation has been developed and applied to multichannel EHG recordings for action-potential (AP) conduction velocity (CV) estimation [8,10,12]. Meanwhile, the direction of propagation has been defined by the incidence angle with regard to the vertical axis of the electrode grid [10]. The delay estimators which can identify EHG propagation direction between each pair of electrodes are based on cross-correlation or cross-coherence analysis [13–15], a spectral matching method [16] or the center of mass calculation of the EHG burst envelope [5]. However, each of these methods is based on the assumption of a linear propagation of EHG between electrodes, which may not be suitable for the EHG signal that is likely to contain also non-linear propagation pattern [5,17,18].

The directed information (DI) process, which measures the amount of information that flows from one process to the other [19], is capable of exploring both linear and nonlinear causality relationships. The major advantages of DI are its model-freeness, unlike the Granger causality, and wide applicability to different types of physiological data, including electrophysiological recordings [20–25]. For example, the potential of DI measures in terms of identifying causal influence of electrical connectivity between brain regions has been reported in recent years [20–24]. Our preliminary work demonstrated the potential use of DI in the study of EHG recordings [26]. However, so far, there is no scheme for DI estimation that has been assessed thoroughly for investigating the propagation of human EHG recordings. To realize this, the reliability and adaptability of the DI-based algorithm should be scientifically studied.

In this paper, we demonstrated the step-wise development of an estimation scheme of information transfer direction between paired EHG electrodes. The reliability of a DI-based algorithm was assessed, and its adaptive parameters were investigated, using simulated data. Thereafter, its applicability was tested using existing raw datasets of multichannel EHG recordings from human subjects. In doing so, we also sought to reveal information on the direction of EHG AP propagation utilizing a novel propagation terminal zone (PTZ) identification method. The PTZ approach was created to compare the significance of surround-inward flow regarding each electrode. This, in turn, enabled us to develop a regional identification of information flow termination (RIIFT) method, and apply it, for the first time, to multichannel EHG signals to establish new biophysiological information on the spatiotemporal nature of electrical excitation of the human uterus.

2. Materials and methods

2.1. Estimation of directed information

The conditional entropy of A given B is defined as

$$H(A|B) = E_{A,B}[-\log p(A|B)], \tag{1}$$

which measures the average prediction error on A given the observation of B. Throughout, we use capital letters for random variables and lowercase letters for their realizations. We denote the sequence of the first i sources from data $X_1, X_2, \cdots$ as $X^i = [X_1, X_2, \cdots X_i]$. The directed information from a random sequence X^n to another random sequence Y^n is defined as

$$I(X^n \to Y^n) \triangleq \sum_{i=1}^{n} I(X^i; Y_i \mid Y^{i-1}) = H(Y^n) - H(Y^n \parallel X^n), \tag{2}$$

where $H(Y^n) = \sum_{i=1}^{n} H(Y_i|Y^{i-1})$ is the entropy of Y^n and $H(Y^n \parallel X^n) = \sum_{i=1}^{n} H(Y_i|Y^{i-1}, X^i)$ is the causally conditional entropy [27]. According to the interpretation of conditional entropy, the directed information from X^n to Y^n defined as (2) measures the improvement in the prediction of Y_i given the past samples Y^{i-1}, when samples X^i are also available.

In this study, we use one of the estimators of the directed information rate $\bar{I}(X^n \to Y^n) = \frac{1}{n} I(X^n \to Y^n)$ introduced in [28], which is defined as:

$$\hat{I}(X^n \to Y^n) \triangleq \frac{1}{n} \sum_{i=1}^{n} D_{KL}(Q(y_i \mid x^i, y^{i-1}) \parallel Q(y_i \mid y^{i-1})), \tag{3}$$

where $D_{KL}(p \parallel q) = E_p[\log \frac{p(x)}{q(x)}]$ is the relative entropy between probability distributions $p(x)$ and $q(x)$ and $Q(y_i \mid y^{i-1})$ denotes the estimate of the conditional probability mass function of y_i given the observation y^{i-1}. This is estimated by the Context-Tree Weighting (CTW) algorithm [28,29]. The depth of the context tree D indicates the memory of the model, i.e., the number of past samples included in the sequences x^i and y^{i-1} in (3). Note that one only needs to estimate the distribution $Q(x_i, y_i \mid x^{i-1}, y^{i-1})$ since the distribution $Q(y_i \mid x^i, y^{i-1})$ is obtained as $Q(y_i \mid x^i, y^{i-1}) = Q(x_i, y_i \mid x^{i-1}, y^{i-1}) / \sum_{y_i} Q(x_i, y_i \mid x^{i-1}, y^{i-1})$. The estimator $\hat{I}$ in (3) is always nonnegative.

2.2. Direction discrimination

The information flow of signal S between channel i and j was defined to be inward to channel i if the factor used for direction discrimination between two channels, $\Theta(j \to i) = \bar{I}(S_j^n \to S_i^n) - \bar{I}(S_i^n \to S_j^n)$, is larger than Θ_s, above which the absolute values of $\Theta(j \to i)$ are regarded as significant.

In order to identify values of $|\Theta(j \to i)|$ that can be regarded as significant, we first evaluated (3) on two independent white noise processes. The absolute values of $\Theta(j \to i)$ corresponding to 10,000 different pairs of source and destination were then calculated. Finally, a one-tailed test, where the pre-specified significance level was set to 5%, was used and the values larger than Θ_s were determined as significant. It is worth noting that Θ_s varies with the change of value of parameters involved in DI estimation.

2.3. Assessment of DI-based algorithm reliability using simulated data

To assess the reliability of the DI-based algorithm for estimating the direction of information flow between two neighboring channels, it was initially tested with the use of simulated signals. The simulated surface EHG signal associated to the uterine contraction, which is between $0.1 - 0.8$ Hz [30,31], was gener-

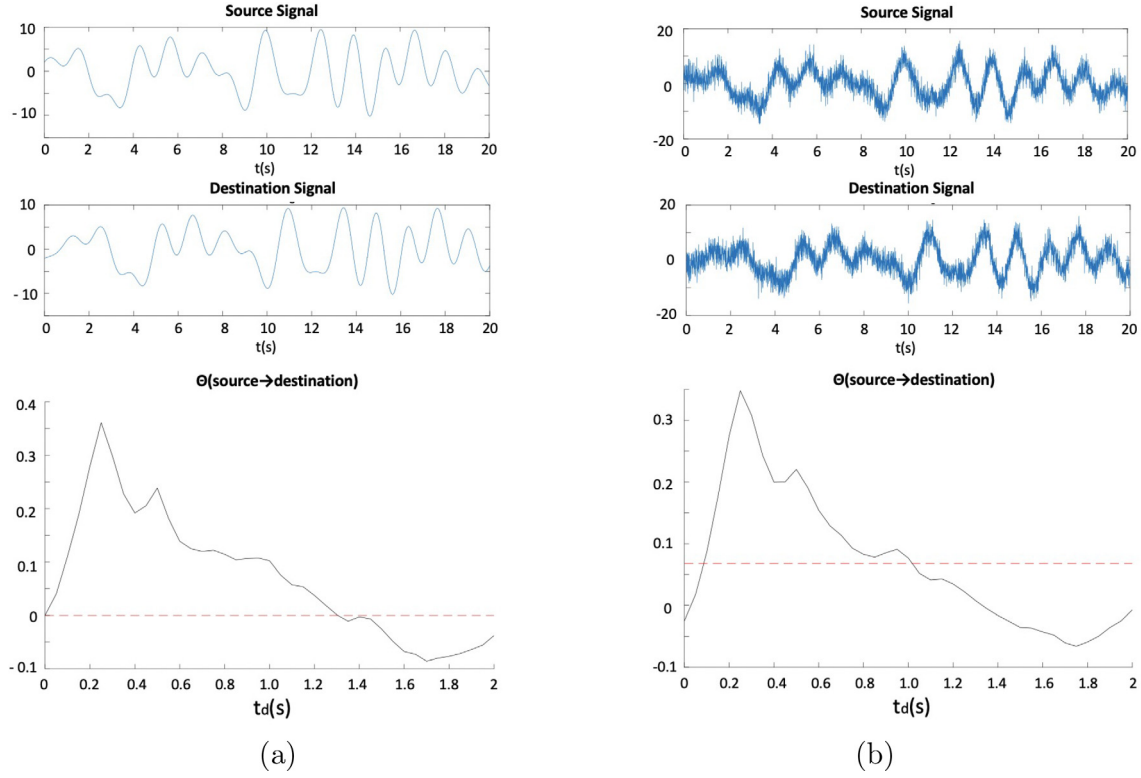

Fig. 1. Plots obtained using simulated data for the investigation of how Θ(source → destination) changes with the time delay from the source to the destination in two cases. (a) Simulated APs without additional noise. (b) Simulated signals with additional Gaussian white noise added to the source and destination. The significant values of Θ(source → destination) were above the threshold Θ_s, which was indicated by the red dashed lines. Corresponding examples of simulated source signal and destination signal delayed by 1 s are shown in the top plots. (For interpretation of the references to colour in this figure legend, the reader is referred to the web version of this article.)

ated by summing the sinusoidal components of frequency f_i with random phases, where $f_i = 0.01 \times i$ $(i = 1, 2, \ldots 80)$ Hz. The sampling frequency is set to 200 Hz to coincide with the sampling frequency of physiological EHG signal used in this study. Its amplitude was then modulated by a Hanning window of 40-second length. The signal was artificially delayed (between 0 s and 2 s) to generate the signal of destination. Pseudorandom noise with normal distribution was added to both source and destination signals, respectively.

The simulated EHG segments of 20-second length were then used in this study to coincide with the estimation on physiological data. Fig. 1 shows how the direction discrimination factor, Θ(source → destination), changes with the time delay t_d from the source to the destination. Without additional noise, the values above zero indicate correct identification of the direction of information flow (*i.e.* from the source to the destination). As shown in Fig. 1(a), accurate results could be obtained when the delay of EHG signal between two channels was no more than 1.3 s as indicated by the red dashed line. In the cases with added noise to the source and destination channels, a new threshold (see Section 2.2) was taken into consideration, the values above which indicate correct identification of direction (Fig. 1(b)). Gaussian white noise was added to the source and destination channels, contributing to 6 dB signal-to-noise ratio (SNR), which was the mean value of the SNR distribution obtained from a previous study [10]. Compared to the case without additional noise, the accurate result in this case was obtained within a narrower range of time delay (approximately between 0.1 s and 1 s) between the source and destination. It is worth noting that the linear propagation model was used specifically for determining the parameters in Section 2.4 which would be difficult if including the non-linear behavior in the models.

2.4. Determination of adaptive DI parameter using simulated data

Further, using the simulated EHG segments (SNR = 6 dB), the parameters of the DI-based algorithm, i.e. the factor of down-sampling *ds*, the depth of context-tree *D* and the way for discretization, were determined. In order to minimize the storage and computational complexity, the EHG segments were down-sampled by a factor *ds* [29]. In this way, the past activity of any sequence X^n considered in the estimation can include $\{x_{n-ds}, x_{n-2\times ds}, \ldots, x_{n-D\times ds}\}$. This assumed that the current activity at an EHG channel does not depend on more than $t_p = D \times ds/F_s$ of past activity at this and the other channels, where F_s is the sampling frequency. To reduce the variance of the DI rate, the DI-based algorithm was applied to all the possible down-sampled sequences $X^n_{(k)} = \{x_{n-k}, x_{n-ds-k}, x_{n-2\times ds-k}, \ldots\}$, $k = 0, 1, 2 \ldots ds - 1$, and the DI rate was obtained by averaging over all $X^n_{(k)}$. We compared four pairs of values of *D* and *ds* (*i.e.* $D = 8$, $ds = 50$; $D = 5$, $ds = 50$; $D = 6$, $ds = 40$; $D = 8$, $ds = 30$) as shown in Fig. 2(a). Several points should be kept in mind when selecting the values of *D* and *ds* in relation to our later analyses of human EHG data:

1) Although the down-sampling was introduced to reduce the computational complexity, the factor *ds* should not be too large such that the main components corresponding to pregnancy contraction (0.1 - 0.8 Hz) be rejected.

2) According to the distance between a pair of neighboring electrodes used in our later analyses, 1.75 cm on the longitude and latitude grid line and 2.47 cm along the diagonal, as well as the estimated CV of EHG signals during excitation-contraction coupling events (ranging from 2.18 to 8.65 cm/s [5,8,10,12,32]), the time it takes for the EHG signal to transmit from a channel to its neighbor was assumed to be within the range 0.29 to 1.13 s. Therefore, t_p should be larger than 1.13 s.

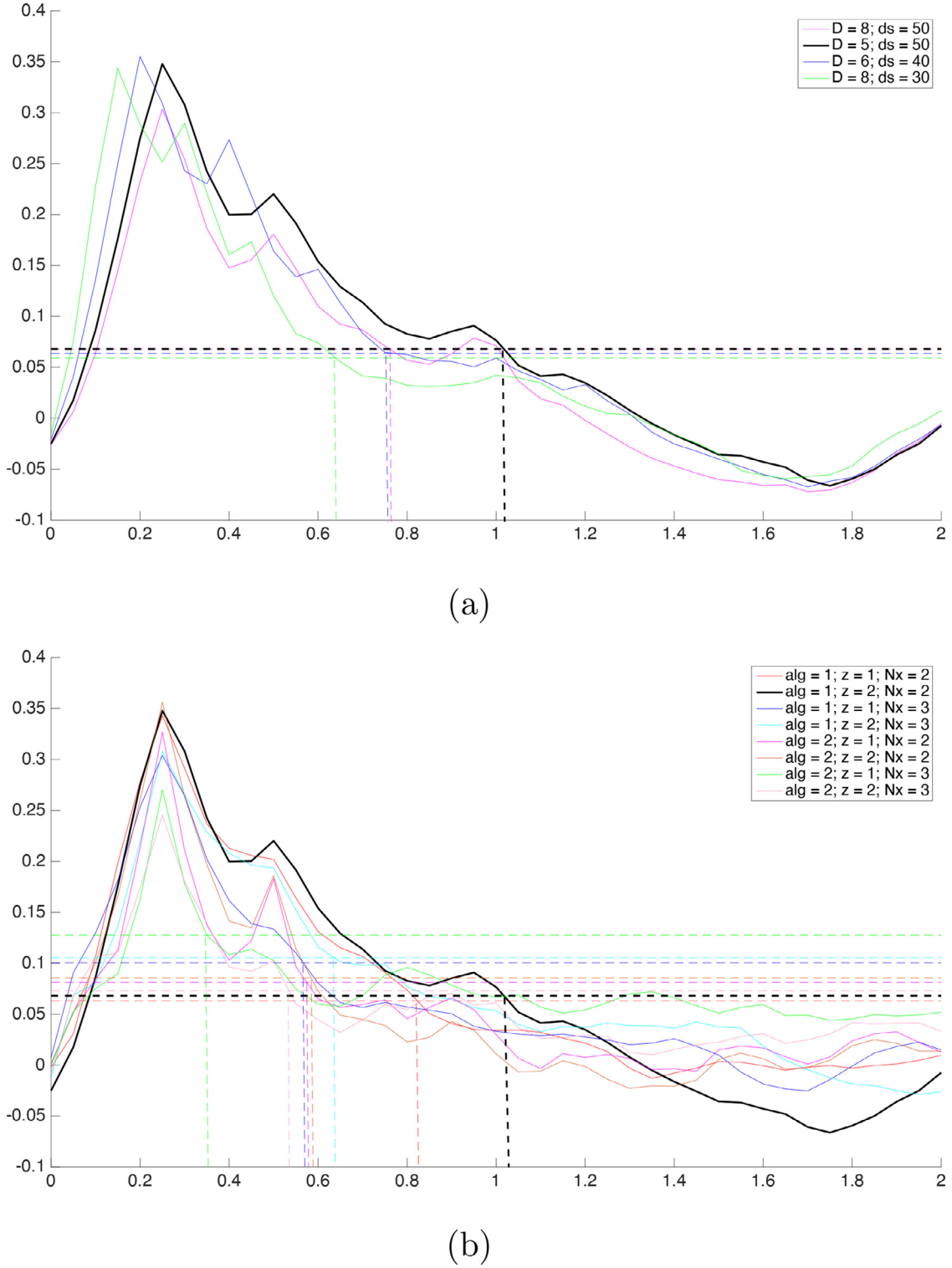

Fig. 2. Comparison between Θ(source → destination) obtained from different settings of parameters involved in DI-based algorithm: (a) the factor of down-sampling *ds* and the depth of context-tree *D*; (b) different ways of discretization. The factors considered in discretization include: 1) the form of samples, which can be the original form ($alg = 1$) or the first-order difference between successive samples ($alg = 2$); 2) the number of counterparts for discretization, which can be 2 ($N_x = 2$) or 3 ($N_x = 3$); 3) the binning method, either the Equal Width Binning method ($z = 1$) or the Equal Frequency Binning method ($z = 2$). The dashed lines represent to corresponding threshold Θ_s and upper boundary of delay for accurate result. Note that since the minimum propagation time of EHG from one channel to its neighbor is assumed to be 0.29s, where Θ(source → destination) increases above the threshold in all cases, there is no need to consider the lower boundary of the delay. The best performance among different cases was indicated by the thick black curves, which covers most of the assumed range of delay (*i.e.* 0.29 - 1.13 s) between two neighboring channels.

3) The larger the value of D is, the greater the computational complexity becomes.

We can observe from Fig. 2(a) that when $D = 5$ and $ds = 50$ (black line), the performance of DI-based algorithm is best among these cases, which accepts the longest delay between two channels. Also, in this way, the acceptable range of delay, where the curve is above the corresponding threshold, covers most of the assumed range of delay (*i.e.* 0.29 - 1.13 s) between two neighboring channels in our later analyses.

After the values of D and ds had been selected, the most adaptive way for discretization, which is used to generate the finite alphabet for probability assignment, was explored (see Fig. 2(b)). The discretization transforms numerical variables into categorical counterparts. The factors involved in the discretization include the form of samples, the number of counterparts and the binning method. Specifically, we computed the discrete derivative of the EHG signals by looking at either the original values of EHG samples ($alg = 1$) or the first-order difference between successive EHG samples ($alg = 1$). The samples were transformed into several counterparts by the means of binning methods. The size of alphabet depends on the number of counterparts for discretization. Although originally the size of alphabet for the CTW algorithm is 2 ($N_x = 2$) [29], we compared it to a larger alphabet ($N_x = 3$) [33] to explore if larger alphabet would perform better in this study. Two commonly used binning methods were compared, *i.e.*, the Equal Width Binning method ($z = 1$) and the Equal Frequency Binning method ($z = 2$) [34].

The thresholds Θ_s were determined by the method described in Section 2.2 using corresponding settings of the factors described above for DI estimation between independent white noise processes. After considering all combinations of different settings of these three factors in Fig. 2(b), it was observed that the best result which accepts the longest delay was obtained when we computed the discrete derivative of the EHG signals by looking at the original values of EHG samples ($alg = 1$) and then transformed them into two counterparts ($N_x = 2$), using the Equal Frequency Binning method ($z = 2$) [34]. These determined parameters will be used for further investigation with the physiological EHG signals.

2.5. Physiological database and EHG data preprocessing

The Icelandic 16-electrode EHG database [35] was used for investigating the direction of UC. The 16-channel EHG signals were recorded from 45 pregnant women using a 4×4 monopolar electrode grid placed on the surface of abdomen as shown in Fig. 3. The distance between the centers of neighboring rows or columns was 17.5 mm. The third column of electrodes (electrodes 9 to 12) was desired to be placed on the median axis of the uterus with the 10th-11th pair of electrodes half way between the uterine fundus and pubic symphysis. Signals were passed to a digital converter and sampled at 200 Hz and filtered by an anti-aliasing filter with high cut-off frequency of 100 Hz. External tocodynamometry (TOCO) was recorded simultaneously from the abdomen.

Recordings used for the study were performed during the third trimester of pregnancy (112 recordings; 16 channels of EHG for each recording) with the average duration of 61 minutes. Two to seven recordings were obtained for each participant at different gestational weeks during the same pregnancy. A detailed description of the experiments for data collection can be found in [35]. For the current data analysis, two clinicians were asked to independently identify the UCs in accordance with the TOCO signal and UC annotation [36]. Only those identifications with full agreement of the two clinicians were used as reference information for identifying UC activities with associated EHG signals.

The wavelet transform using *Daubechies db7* wavelet was applied to each recording for separating the UC component from the other components which are regarded as noise in this study. Instead of considering the whole frequency range of main components of EHG activities (0.1 - 3 Hz), we filtered the EHG signals to keep only the low-frequency components (0.1 - 0.8 Hz), in order to discard the maternal and fetal ECG as much as possible and cover the components by which the pregnancy contraction can be mainly represented [10,30,31,37]. Furthermore, the baseline interference was eliminated by using a median filtering whose order was set to 1000.

The analyzable EHG segments were then selected using the TOCO-identified UCs as reference. Only those segments with corresponding analyzable EHG signals from all 16 electrode array channels were taken into account for further analysis. The diagram of EHG segment selection is shown in Fig. 4. An example of 16-channel filtered EHG signals and corresponding TOCO recording is shown in Fig. 5, where the selected analyzable EHG segments are indicated by the dashed red frames.

Next, for these analyzable segments, the UC-associated EHG peaks were identified by averaging EHG signals over 16 channels. The preprocessed EHG segments from each of the 16 channels were then obtained by applying the windows of 20-second length that began 10 s before, and ended 10 s after, the time instant corresponding to the UC-associated EHG segment peaks. In this way, it was ensured that the APs involved in the estimation have reached their termination. An example of an analyzable EHG segment can be observed in Fig. 6. Finally, a total of 79×16 analyzable segments from 25 recordings were selected to determine the propagation terminal zone (PTZ) of EHG signal.

2.6. EHG propagation terminal zone identification algorithm

The PTZ of EHG signals was defined in this study as the location in the plane of uterus towards which the information flow terminated. The identification algorithm was proposed, specifically, for electrode configuration of M-by-N grid ($M \geq 3$, $N \geq 3$; for this study, $M = N = 4$), where each electrode has at most 8 neighbors. Hence, the significance of surround-inward flow of causal information towards electrode i in terms of a specific UC can be calculated as follow:

$$\alpha(i) = \frac{1}{8}\left(\sum_{j \in A_i} \left(\frac{1}{2} + \frac{\Theta(j \to i)}{2|\Theta(j \to i)|} \right) + \frac{1}{2} \times (8 - n_r) \right), \tag{4}$$

where A_i is the aggregate consisting of all neighboring electrodes of electrode i and n_r is the number of elements in A_i. When the value of $|\Theta(j \to i)|$ is smaller than Θ_s, $\Theta(j \to i)$ is set to zero. The additional $8 - n_r$ model neighboring electrodes were introduced to estimate α for the electrodes on the edges of grid. Fifty-percent potential of inward flow was assumed towards the estimated electrode from each of its model neighbors. This appears as the last term on the right side of 4) as a moderating factor. In this way, it would be consistent for all the electrodes when estimating the inward flow of information to an electrode from its neighboring electrodes. According to the values of α of $M \times N$ electrodes, the PTZ within the area of electrode grid was finally determined by the position of electrode corresponding to the largest value of α. Intuitively, activity at the PTZ electrode is driven by the activity at the other electrodes via causal interactions. The PTZ is thus expected to be the destination of UCs, where there are strongest incoming causal connections.

3. Results

From 25 recordings (*i.e.* Rec01 - Rec25) there were 79 UCs with interpretable EHG segments from all 16 channels used for the PTZ identification of the surface AP within the estimated area

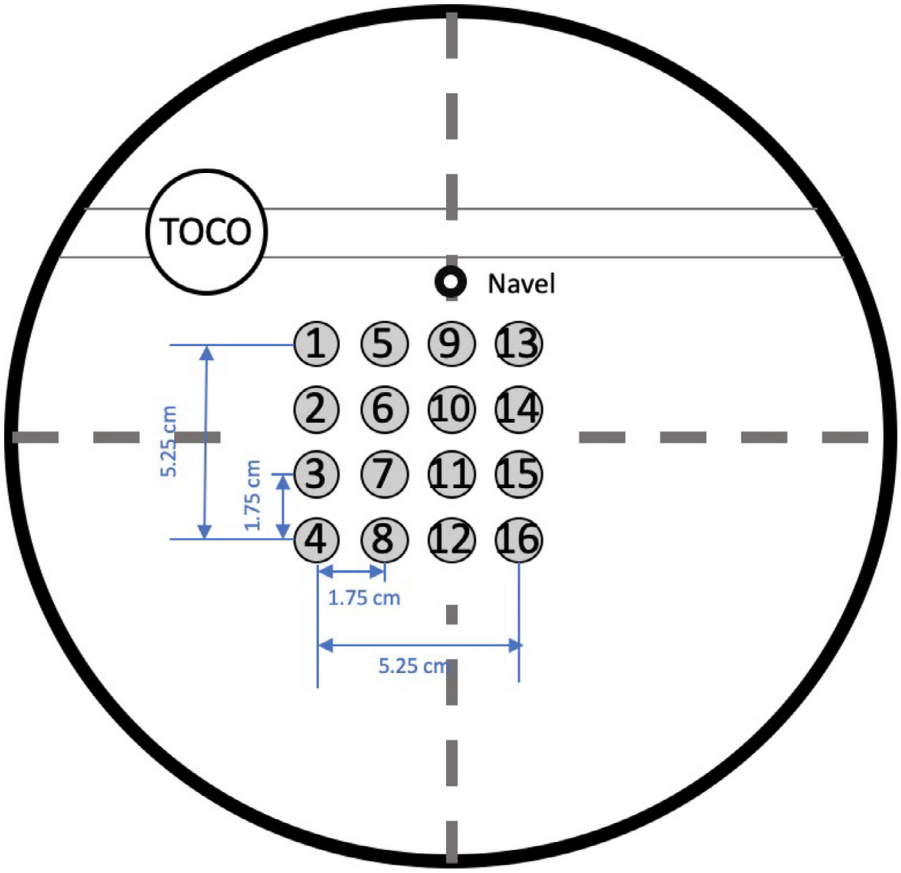

Fig. 3. The estimated area on the abdomen is within the position of 4×4 electrode grid. The third column of electrodes is expected to be placed on the medial axis of uterus represented by the vertical dashed line and the horizontal dashed line between the second and third rows of electrode grid represents the half way between the uterine fundus and pubic symphysis [35].

on the abdomen corresponding to the electrodes of a $4-by-4$ grid (Fig. 3). An example of the filtered 16-channel EHG signals for Rec02 is shown in Fig. 5, where 6 UCs were considered.

The PTZ was obtained by estimating the significance of surround-inward flow of information of each channel using the estimator α in (4). Table 1 summarizes the PTZ electrode identified for each UC by the method of RIIFT. For 57 out of 79 UCs (*i.e.* 72.15% of total cases), the determined PTZ electrodes were along the third column, which was desired to be placed on the median axis of the uterus, avoiding the navel. Among these, 44 UCs (*i.e.* 55.70% of total cases) had their estimated PTZ at electrodes 10 or 11, which were expected to locate in the middle between the uterine fundus and pubic symphysis. For 13 UCs, the PTZ was identified corresponding to the 9th or the 12th electrode, which is in the third column, but not in the middle of it. The PTZ was identified corresponding for the second or the fourth column of electrodes for 21 cases. There was only one PTZ obtained farther away in the first column. It can also be observed from Table 1 that, for the recordings with more than one UCs, the PTZ was often identified in a same column or even corresponding to the same electrode. However, this was not always the case.

Fig. 7 compares the percentage of cases where the PTZ were identified corresponding to each electrodes of the grid, showing the desired position of electrode grid on the abdomen of the pregnant women. The most probably identified PTZ within the recording area on abdomen of the 79 cases is shown clearly in Fig. 7.

Fig. 8 shows some examples of the cases in Table 1, where the PTZ is identified on the third column of electrodes. The values of $\alpha(i)$ corresponding to each electrode are represented by different colors. In order to have a clearer view of the flow direction of information of EHG within the electrode grid, additional points were interpolated between each pair of neighboring channels using cubic interpolation method to increase the resolution. We can observe in Fig. 8 that how α changes within the recording area, as well as the PTZ region where the highest value of α is obtained. For example, in Fig. 8(c), the warmest color is observed in the area below and nearby the intersection point of vertical and horizontal dashed lines, which indicates the PTZ at the location of electrode 11. The color turns colder radially, which shows obvious flow inward to the PTZ.

4. Discussion

RIIFT uses, as a basis, the estimation of DI to infer the causal interactions between recordings at EHG channels, via which the activities at the destination channels are driven by the activities at the source channels. As we demonstrate here, RIIFT can be applied to investigate the likely termination point of APs, estimated within the confines of the recording area, using the multielectrode array data. The parameters involved in the estimation are determined according to the results from previous EHG measurements. For example, the parameters of the DI-based algorithm were valued considering the estimated CV of EHG observed in the previous publications. Also, the length of preprocessed EHG segment was decided by considering the minimum duration of burst [5,7,8,10,12,32].

This is the first time that DI estimation has been applied to the analysis of spatiotemporal electrical excitation in the human uterus. It has been considered previously in the electrophysiological studies of brain network to investigate EEG propagation, which paves the way for the development of novel nonsurgical treat-

Table 1
PTZ electrode identified by RIIFT method for each UC.

Recording	UC	C1				C2				C3				C4			
		e1	e2	e3	e4	e5	e6	e7	e8	e9	e10	e11	e12	e13	e14	e15	e16
Rec01	01											✓					
	02							✓									
	03							✓									
Rec02	04												✓				
	05						✓										
	06											✓					
	07												✓				
	08															✓	
	09											✓					
	10								✓								
Rec03	11														✓		
	12											✓					
	13											✓					
	14												✓				
	15												✓				
Rec04	16											✓					
	17											✓					
	18						✓										
	19												✓				
Rec05	20						✓										
	21											✓					
	22												✓				
	23						✓										
	24										✓						
	25						✓										
Rec06	26											✓					
	27										✓						
	28															✓	
Rec07	29										✓						
	30											✓					
Rec08	31											✓					
	32										✓						
	33										✓						
Rec09	34									✓							
	35										✓						
	36											✓					
	37											✓					
	38							✓									
Rec10	39												✓				
	40											✓					
	41											✓					
	42											✓					
Rec11	43											✓					
	44											✓					
	45								✓								
Rec12	46												✓				
	47											✓					
	48										✓						
Rec13	49												✓				
	50											✓					
	51	✓															
Rec14	52						✓										
Rec15	53							✓									
Rec16	54											✓					
Rec17	55							✓									
	56							✓									
Rec18	57										✓						
	58												✓				
Rec19	59											✓					
	60											✓					
Rec20	61												✓				
	62											✓					
Rec21	63										✓						
	64											✓					
Rec22	65										✓						
	66							✓									
	67											✓					

(*continued on next page*)

Table 1 (*continued*)

Recording	UC	C1				C2				C3				C4			
		e1	e2	e3	e4	e5	e6	e7	e8	e9	e10	e11	e12	e13	e14	e15	e16
	68															√	
	69											√					
	70								√								
Rec23	71										√						
	72											√					
	73												√				
	74											√					
	75										√						
	76											√					
Rec24	77											√					
	78											√					
Rec25	79						√										

C1 - C4: the 1st to the 4th columns of the electrode grid; e1 - e16: the 1st to the 16th electrodes.

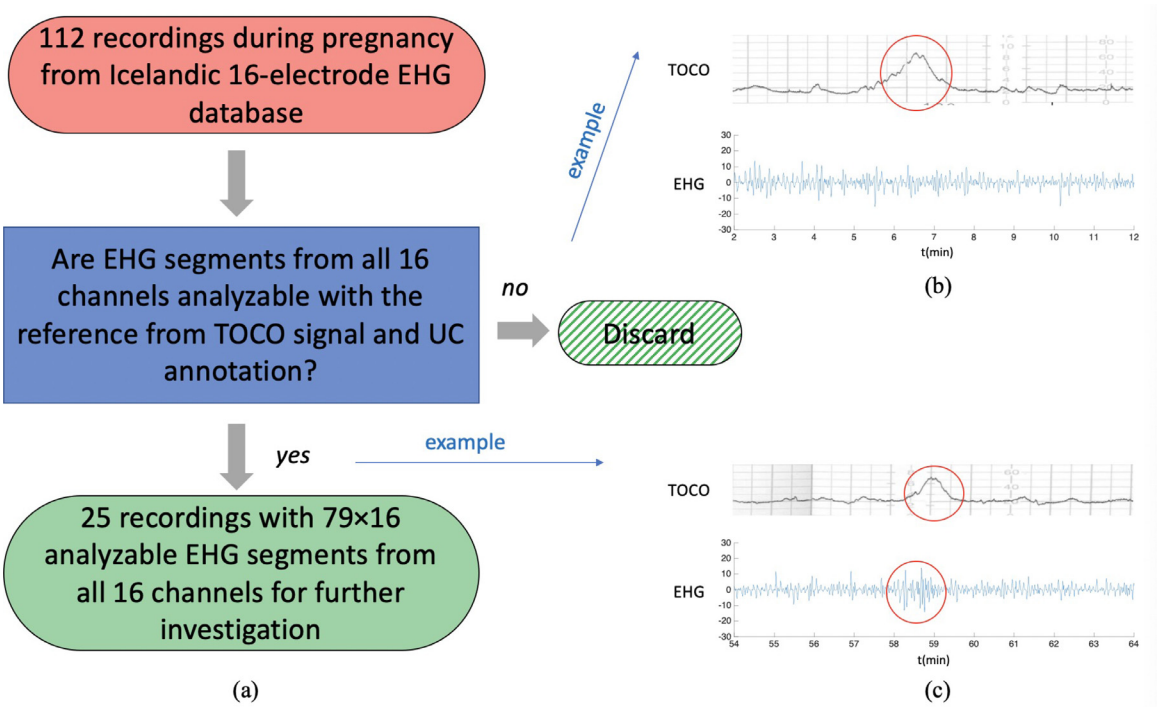

Fig. 4. Diagram to illustrate the selection of EHG segments. (a) 25 recordings with 79×16 segments were selected from 112 recordings as analyzable to be investigate further. (b) Example of EHG segment of which there is corresponding TOCO-identified UC but is not analyzable. (c) Example of analyzable EHG segment.

ments for the diseases such as epilepsy and Parkinson's disease [20–24]. Since there is not a commonly used non-linear model of EHG propagation, we used the linear propagation model in this study to assess the reliability of the DI-based algorithm and to determine the adaptive DI parameters. As a principled tool from the information theory, DI has a model-free nature. Hence, when then applied to the real physiological data, DI has the ability to capture both linear and non-linear behaviors. The results obtained by RIIFT are reliable only when the distance between neighboring electrodes is within an acceptable range (as is the case with 16 electrode array of the Icelandic dataset used in this study) in part due to resolution of current EHG signals as well as the CV being estimated to be as low as 2.18 cm/s [5,8,10,12,32]. This prevents us from estimating EHG propagation by RIIFT using another database if obtained by a bespoke eight-electrode system where the distance between neighboring electrodes can be up to 8 cm [38,39]. Using the Icelandic dataset, the resulting identified PTZ within the estimated area in this study is obtained in the third column of electrodes in most cases (Table 1), indicating that during pregnancy, surface APs propagate to the media axis of uterus within the recording area. Moreover, the PTZ electrodes of more than half of the UCs are shown in the middle of the third column, indicating that the information flow of pregnancy contraction in this area is inward to the center, likely, between the uterine fundus and pubic symphysis along the medial axis. However, these results were obtained from only a small region. In the clinical setting, the Icelandic 16-electrode EHG database was obtained using the electrode grid which covered $5.25\ cm \times 5.25\ cm$ area measured by the center of each electrode. While this facilitates minimizing discomfort and intrusion to the pregnant women, and has enabled us to advance our understanding of important features of spatiotemporal electrical excitation of uterine contractions, this comes with limitations. For example, there may be other PTZs that occur away from the recording electrode array which cannot be identified by the current settings. This possibility was suggested by the data obtained from a 151-channel electromagnetic sensor array developed to evaluate a multiscale electromagnetic forward model of human myometrial contractions [40]. Another limitation is that, in this scenario it is difficult to extrapolate detailed information regarding the source and path of EHG propagation. Instead, therefore, we focused on de-

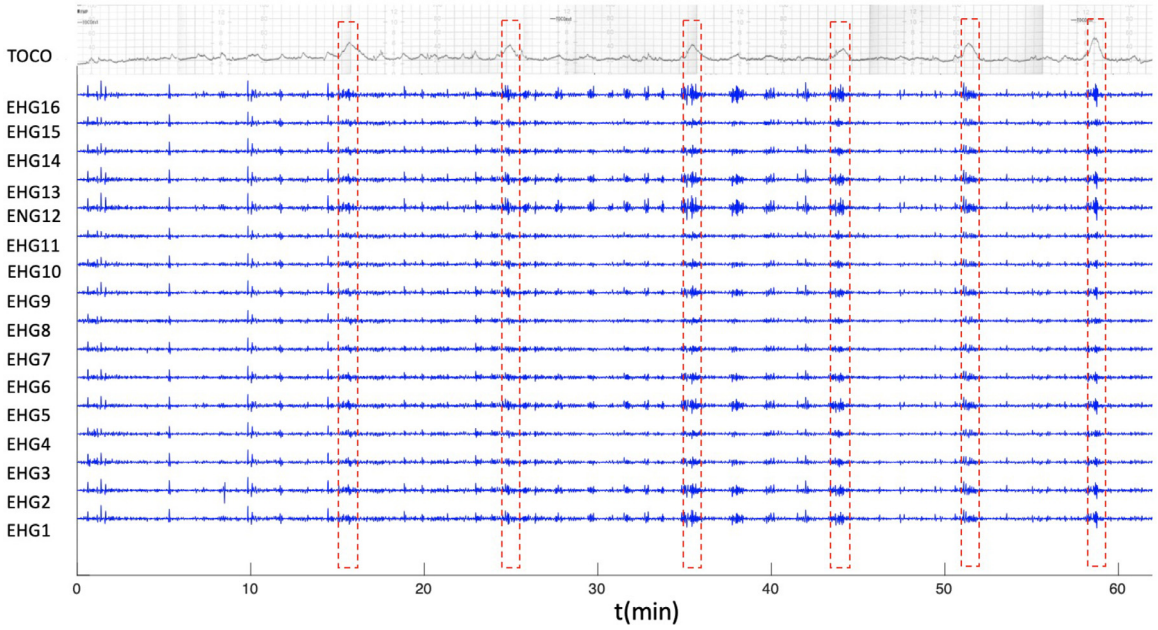

Fig. 5. Example of the 16-channel filtered EHG signals. The identified UC-associated fluctuations are circled by the dashed red frames. (For interpretation of the references to colour in this figure legend, the reader is referred to the web version of this article.)

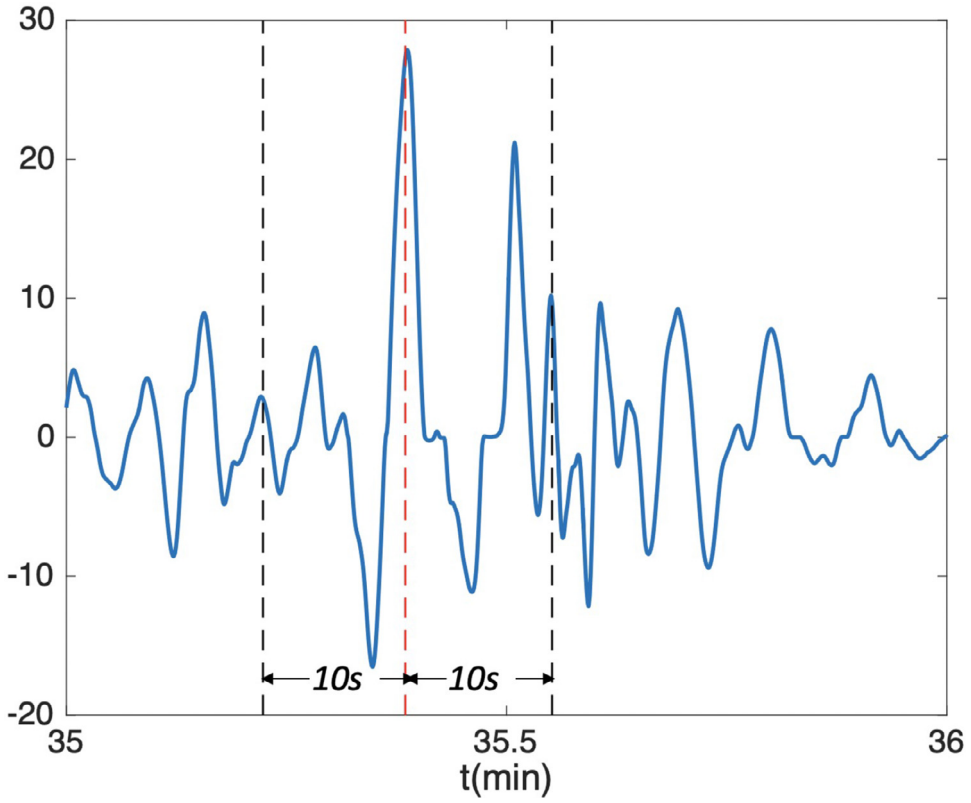

Fig. 6. Illustration of EHG segmentation. The EHG signal that is averaged over 16 channels is used for identifying the UC-associated EHG peaks. The time instant of EHG peak is indicated by the dashed red line. The preprocessed EHG segments from 16 channels were obtained by a window of 20-second length represented by the dashed black lines. (For interpretation of the references to colour in this figure legend, the reader is referred to the web version of this article.)

termining the probabilities of spatial termination of APs within the estimated area and report that the APs propagate towards the center of uterus plane within the recording area (*i.e.* the middle part of uterus) during pregnancy.

Many previous studies investigating the propagation of UC-associated electrical activity, which focused on its source, direction and/or velocity, have indicated that the electrical activity of UCs could originate from more than one location on the uterus and propagate in different directions [5,10,12,15,16,18,41]. Our analysis is consistent with these suggestions with the added identification of preferential sites of excitation termination. However, while indeed, various directions of EHG propagation have been

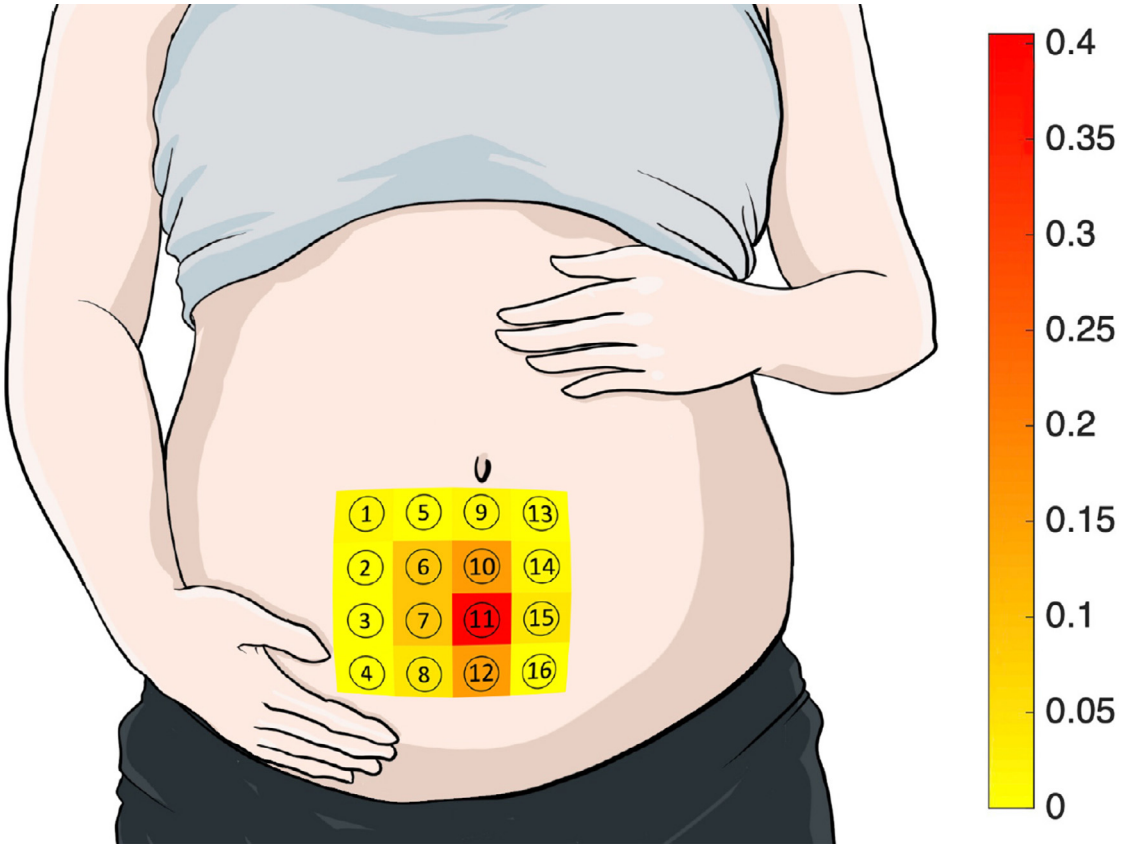

Fig. 7. The probability of PTZ electrodes shown on the desired position of abdomen identified for the estimated UCs. The circles with number represent the corresponding electrodes, composing the 16-channel electrode grid (5.25 $cm \times 5.25$ cm measured by the center of each electrode) used for EHG recording (see Fig. 3). The color represents the percentage of cases where the PTZ is identified corresponding to the electrode.

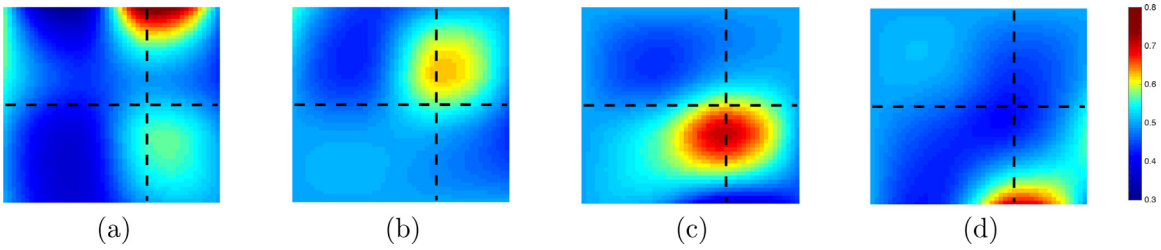

Fig. 8. Examples of four individual cases where the PTZ was identified on the third column of electrodes. The dash lines in this figure correspond to the dash lines in Fig. 3. Specifically, the vertical dashed line corresponds to the third column of electrodes (electrodes 9 to 12), which was desired to be placed on the median axis of uterus. The horizontal dashed line corresponds to the middle line of electrode grid between the second and third rows, which was desired to be placed in the center between the uterine fundus and pubic symphysis. The color represents the value of α. The higher the value is, the more significant the surround-inward flow of information of corresponding area is. The PTZ is identified corresponding to (a) the $9th$ electrode, (b) the $10th$ electrode, (c) the $11th$ electrode and (d) the $12th$ electrode, respectively.

suggested, including: 1) top down [8,16,18] 2) upward and downward [5,41] and 3) no preferred direction [12]. The identified preferential sites of excitation termination in our study revealed not only the possible simultaneous upward and downward propagation during the pregnancy period, but also the preferred horizontal direction of propagation, *i.e.* toward the median axis of the uterus. This can also illustrate that the source may locate on different sites of the uterus. Nonetheless, the AP terminations identified in this study exhibit variation within the same recording. This indicates, in turn, some variation in the propagation direction of APs, and/or the possible low synchronization of uterine electrical activities or the inhomogeneous structure of uterus [42–45]. As the PTZ illustrates the propagation of electrical activity, to some extent, one may speculate that differences of its location may occur between normal and abnormal uterine activation thereby informing clinical diagnosis for pregnancy complications. This requires further investigation on the EHG signals recorded from patients at risk of, or already diagnosed with, relevant diseases (*i.e.* spontaneous preterm labor). Future work should focus on examining any variation of EHG propagation during different gestations and periods of labor.

In order to achieve better understanding of EHG propagation direction, given the limitations involved in the current available databases regarding their low resolution of EHG signals, the establishment of a new database of recordings should be considered. Ideally this would be furnished with data obtained utilizing a greater number of electrodes with higher signal detection performance appropriate to RIIFT analysis and covering a larger area of uterus. This requires future work to be focused on developing advanced EHG recording devices and accompanying analysis tools (such as that described herein).

Also, we lack the knowledge of the topology of the uterus - it could be that part of the uterine wall is closer to a sub-

dermal layer of skin at these positions compared to others, which may affect signal fidelity in a manner that influences information flow. Hence, in future experiments, electrode array positioning and recording could be optimized with information obtained with the aid of sub-dermal imaging techniques, *e.g.*, ultrasound [46]. It is possible that positioning electrodes close to the median vertical axis is beneficial for the SNR during contraction due to the change in conducting volume induced by the movement of the uterus during contraction [47]. In this study, we did not consider the conducting volume effect since the EHG signals were obtained using the electrode grid which covered only a small area of pregnant uterus, where we believe the conducting volume effect would not be substantial.

Continued advances in such a relatively non-invasive recording approach is required to improve our biological and clinically-relevant understandings of how electrical excitation controls human uterine contractile function (relevant to the onset timing, periodicity of events and strength of contractions). In particular, a better understanding of AP propagation direction is a prerequisite to enable the utilization of these features for clinical implementation, thereby achieving diagnosis of dysfunction in pregnancy and labor, *e.g.*, preterm birth or dystocia at term.

5. Conclusion

In summary, we have developed a new approach and utilized it to the analysis of in vivo human uterine EHG recordings that reveals preferential spatial regions of termination of propagated electrical signals. This provides an important platform for future, much-needed, studies to fill knowledge gaps in the spatiotemporal patterns of electrical excitation. A combination of this analytical process with new, technologically advanced, experimentation offers the possibility of advancing our understanding, including identification of clinically-relevant features, of human uterine excitability.

Declaration of Competing Interest

I confirm that there are no known conflicts of interest associated with this publication and there has been no significant financial support for this work that could have influenced its outcome.

I confirm that the manuscript has been read and approved by all named authors and that there are no other persons who satisfied the criteria for authorship but are not listed. I further confirm that the order of authors listed in the manuscript has been approved by all of us.

I confirm that we have given due consideration to the protection of intellectual property associated with this work and that there are no impediments to publication, including the timing of publication, with respect to intellectual property. In so doing I confirm that we have followed the regulations of our institutions concerning intellectual property.

Acknowledgment

This research was supported by Bill & Melinda Gates Foundation (OPP1148910), NIHR AI Award (AI_AWARD02312) and the National Key Research and Development Program of China (2019YFC0119700).

References

[1] M.M. Slattery, J.J. Morrison, Preterm delivery, The Lancet 360 (9344) (2002) 1489–1497, doi:10.1016/s0140-6736(02)11476-0.
[2] Y. Xu, H. Liu, D. Hao, M. Taggart, D. Zheng, Uterus modeling from cell to organ level: towards better understanding of physiological basis of uterine activity, IEEE Rev Biomed Eng (2020). 1–1
[3] M.P. Nageotte, W. Dorchester, M. Porto, K.A. Keegan, R.K. Freeman, Quantitation of uterine activity preceding preterm, term, and postterm labor, Am. J. Obstet. Gynecol. 158 (6) (1988) 1254–1259, doi:10.1016/0002-9378(88)90353-5.
[4] N.A. Sathe, F.E. Likis, J.L. Young, A. Morgans, D. Carlson-Bremer, J. Andrews, Procedures and uterine-sparing surgeries for managing postpartum hemorrhage, Obstetrical & Gynecological Survey 71 (2) (2016) 99–113, doi:10.1097/ogx.0000000000000273.
[5] E. Mikkelsen, P. Johansen, A. Fuglsang-Frederiksen, N. Uldbjerg, Electrohysterography of labor contractions: propagation velocity and direction, Acta Obstet Gynecol Scand 92 (9) (2013) 1070–1078, doi:10.1111/aogs.12190.
[6] M. Lucovnik, R.J. Kuon, L.R. Chambliss, W.L. Maner, S.-Q. Shi, L. Shi, J. Balducci, R.E. Garfield, Use of uterine electromyography to diagnose term and preterm labor, Acta Obstet Gynecol Scand 90 (2) (2010) 150–157, doi:10.1111/j.1600-0412.2010.01031.x.
[7] M. Lucovnik, W.L. Maner, L.R. Chambliss, R. Blumrick, J. Balducci, Z. Novak-Antolic, R.E. Garfield, Noninvasive uterine electromyography for prediction of preterm delivery, Am. J. Obstet. Gynecol. 204 (3) (2011) 228.e1–228.e10, doi:10.1016/j.ajog.2010.09.024.
[8] H. de Lau, C. Rabotti, R. Bijloo, M.J. Rooijakkers, M. Mischi, S.G. Oei, Automated conduction velocity analysis in the electrohysterogram for prediction of imminent delivery: a preliminary study, Comput Math Methods Med 2013 (2013) 1–7, doi:10.1155/2013/627976.
[9] J. Alberola-Rubio, J. Garcia-Casado, G. Prats-Boluda, Y. Ye-Lin, D. Desantes, J. Valero, A. Perales, Prediction of labor onset type: spontaneous vs induced role of electrohysterography? Comput Methods Programs Biomed 144 (2017) 127–133, doi:10.1016/j.cmpb.2017.03.018.
[10] C. Rabotti, M. Mischi, S.G. Oei, J.W.M. Bergmans, Noninvasive estimation of the electrohysterographic action-potential conduction velocity, IEEE Trans. Biomed. Eng. 57 (9) (2010) 2178–2187, doi:10.1109/tbme.2010.2049111.
[11] M. Borowska, E. Brzozowska, P. Kuć, E. Oczeretko, R. Mosdorf, P. Laudański, Identification of preterm birth based on RQA analysis of electrohysterograms, Comput Methods Programs Biomed 153 (2018) 227–236, doi:10.1016/j.cmpb.2017.10.018.
[12] L. Lange, A. Vaeggemose, P. Kidmose, E. Mikkelsen, N. Uldbjerg, P. Johansen, Velocity and directionality of the electrohysterographic signal propagation, PLoS ONE 9 (1) (2014) e86775, doi:10.1371/journal.pone.0086775.
[13] H. de Lau, K.T. Yang, C. Rabotti, M. Vlemminx, G. Bajlekov, M. Mischi, S.G. Oei, Toward a new modality for detecting a uterine rupture: electrohysterogram propagation analysis during trial of labor after cesarean, The Journal of Maternal-Fetal & Neonatal Medicine 30 (5) (2016) 574–579, doi:10.1080/14767058.2016.1178227.
[14] M. Domino, B. Pawlinski, Z. Gajewski, Biomathematical pattern of EMG signal propagation in smooth muscle of the non-pregnant porcine uterus, PLoS ONE 12 (3) (2017) e0173452, doi:10.1371/journal.pone.0173452.
[15] B. Karlsson, J. Terrien, V. Gudmundsson, T. Steingrimsdottir, C. Marque, Abdominal EHG on a 4 by 4 grid: mapping and presenting the propagation of uterine contractions, in: 11th Mediterranean Conference on Medical and Biomedical Engineering and Computing 2007, Springer Berlin Heidelberg, 2007, pp. 139–143, doi:10.1007/978-3-540-73044-6_35.
[16] C. Rabotti, M. Mischi, J.O.E.H. van Laar, G.S. Oei, J.W.M. Bergmans, Inter-electrode delay estimators for electrohysterographic propagation analysis, Physiol Meas 30 (8) (2009) 745–761, doi:10.1088/0967-3334/30/8/002.
[17] M.M. Hassan, J. Terrien, C. Muszynski, A. Alexandersson, C. Marque, B. Karlsson, Better pregnancy monitoring using nonlinear correlation analysis of external uterine electromyography, IEEE Trans. Biomed. Eng. 60 (4) (2013) 1160–1166, doi:10.1109/tbme.2012.2229279.
[18] A. Diab, S. Boudaoud, B. Karlsson, C. Marque, Performance comparison of coupling-evaluation methods in discriminating between pregnancy and labor EHG signals, Comput. Biol. Med. 132 (2021) 104308, doi:10.1016/j.compbiomed.2021.104308.
[19] H. Marko, The bidirectional communication theory–a generalization of information theory, IEEE Trans. Commun. 21 (12) (1973) 1345–1351, doi:10.1109/tcom.1973.1091610.
[20] C.J. Quinn, T.P. Coleman, N. Kiyavash, N.G. Hatsopoulos, Estimating the directed information to infer causal relationships in ensemble neural spike train recordings, J Comput Neurosci 30 (1) (2010) 17–44, doi:10.1007/s10827-010-0247-2.
[21] M. Wibral, R. Vicente, J.T. Lizier, Directed information measures in neuroscience, Springer, 2014.
[22] Y. Liu, S. Aviyente, Quantification of effective connectivity in the brain using a measure of directed information, Comput Math Methods Med 2012 (2012) 1–16, doi:10.1155/2012/635103.
[23] R. Malladi, G. Kalamangalam, N. Tandon, B. Aazhang, Identifying seizure onset zone from the causal connectivity inferred using directed information, IEEE J Sel Top Signal Process 10 (7) (2016) 1267–1283, doi:10.1109/jstsp.2016.2601485.
[24] K. So, A.C. Koralek, K. Ganguly, M.C. Gastpar, J.M. Carmena, Assessing functional connectivity of neural ensembles using directed information, J Neural Eng 9 (2) (2012) 026004, doi:10.1088/1741-2560/9/2/026004.
[25] A. Rao, A.O. HERO III, D.J. States, J.D. Engel, Using directed information to build biologically relevant influence networks, J Bioinform Comput Biol 6 (03) (2008) 493–519.
[26] Y. Xu, D. Hao, D. Zheng, Analysis of electrohysterographic signal propagation direction during uterine contraction: the application of directed information, in: 2020 42nd Annual International Conference of the IEEE Engineering in Medicine & Biology Society (EMBC), IEEE, 2020, doi:10.1109/embc44109.2020.9175423.

[27] G. Kramer, Directed Information for Channels with Feedback, Eidgenossiche Technische Hochschule Zurich, 1998 Ph.D. thesis.
[28] J. Jiao, H.H. Permuter, L. Zhao, Y.-H. Kim, T. Weissman, Universal estimation of directed information, IEEE Trans. Inf. Theory 59 (10) (2013) 6220–6242.
[29] F.M.J. Willems, Y.M. Shtarkov, T.J. Tjalkens, The context-tree weighting method: basic properties, IEEE Trans. Inf. Theory 41 (3) (1995) 653–664, doi:10.1109/18.382012.
[30] J. Jezewski, K. Horoba, A. Matonia, J. Wrobel, Quantitative analysis of contraction patterns in electrical activity signal of pregnant uterus as an alternative to mechanical approach, Physiol Meas 26 (5) (2005) 753–767, doi:10.1088/0967-3334/26/5/014.
[31] C. Marque, J.M.G. Duchene, S. Leclercq, G.S. Panczer, J. Chaumont, Uterine EHG processing for obstetrical monitorng, IEEE Trans. Biomed. Eng. BME-33 (12) (1986) 1182–1187, doi:10.1109/tbme.1986.325698.
[32] J.G. Planes, J.P. Morucci, H. Grandjean, R. Favretto, External recording and processing of fast electrical activity of the uterus in human parturition, Medical & Biological Engineering & Computing 22 (6) (1984) 585–591, doi:10.1007/bf02443874.
[33] T.J. Tjalkens, Y.M. Shtarkov, F.M. Willems, Sequential weighting algorithms for multi-alphabet sources, in: Proc. 6th Joint Swedish-Russian Intl. Workshop on Information Theory, Citeseer, 1993, pp. 22–27.
[34] S. Kotsiantis, D. Kanellopoulos, Discretization techniques: a recent survey, GESTS International Transactions on Computer Science and Engineering 32 (1) (2006) 47–58.
[35] A.S. Alexandersson, Icelandic 16-electrode electrohysterogram database, 2014, doi:10.13026/C2159J.
[36] J. Peng, D. Hao, H. Liu, J. Liu, X. Zhou, D. Zheng, Preliminary study on the efficient electrohysterogram segments for recognizing uterine contractions with convolutional neural networks, Biomed Res Int 2019 (2019) 1–9, doi:10.1155/2019/3168541.
[37] C. Rabotti, M. Mischi, L. Beulen, G. Oei, J. Bergmans, Modeling and identification of the electrohysterographic volume conductor by high-density electrodes, IEEE Trans. Biomed. Eng. 57 (3) (2010) 519–527, doi:10.1109/tbme.2009.2035440.
[38] D. Hao, J. Peng, Y. Wang, J. Liu, X. Zhou, D. Zheng, Evaluation of convolutional neural network for recognizing uterine contractions with electrohysterogram, Comput. Biol. Med. 113 (2019) 103394, doi:10.1016/j.compbiomed.2019.103394.
[39] D. Hao, Y. An, X. Qiao, Q. Qiu, X. Zhou, J. Peng, Development of electrohysterogram recording system for monitoring uterine contraction, J Healthc Eng 2019 (2019) 1–9, doi:10.1155/2019/4230157.
[40] M. Zhang, P.S.L. Rosa, H. Eswaran, A. Nehorai, Estimating uterine source current during contractions using magnetomyography measurements, PLoS ONE 13 (8) (2018) e0202184, doi:10.1371/journal.pone.0202184.
[41] T.Y. Euliano, D. Marossero, M.T. Nguyen, N.R. Euliano, J. Principe, R.K. Edwards, Spatiotemporal electrohysterography patterns in normal and arrested labor, Am. J. Obstet. Gynecol. 200 (1) (2009) 54.e1–54.e7, doi:10.1016/j.ajog.2008.09.008.
[42] R.B. Govindan, E. Siegel, S. Mckelvey, P. Murphy, C.L. Lowery, H. Eswaran, Tracking the changes in synchrony of the electrophysiological activity as the uterus approaches labor using magnetomyographic technique, Reproductive Sciences 22 (5) (2014) 595–601, doi:10.1177/1933719114556484.
[43] W.J.E.P. Lammers, The electrical activities of the uterus during pregnancy, Reproductive Sciences 20 (2) (2012) 182–189, doi:10.1177/1933719112446082.
[44] D. Devedeux, C. Marque, S. Mansour, G. Germain, J. Duchêne, Uterine electromyography: a critical review, Am. J. Obstet. Gynecol. 169 (6) (1993) 1636–1653, doi:10.1016/0002-9378(93)90456-s.
[45] W.J. Lammers, K. Arafat, A. el Kays, T.Y. el Sharkawy, Spatial and temporal variations in local spike propagation in the myometrium of the 17-day pregnant rat, American Journal of Physiology-Cell Physiology 267 (5) (1994) C1210–C1223, doi:10.1152/ajpcell.1994.267.5.c1210.
[46] E. Kalafat, O. Karaaslan, Ultrasound anatomy of the uterus at term, in: Intrapartum Ultrasonography for Labor Management, Springer International Publishing, 2021, pp. 35–42, doi:10.1007/978-3-030-57595-3_4.
[47] J. Terrien, S. Rihana, J. Gondry, C. Marque, Modeling the effects of the electrodes position on the surface EMG characteristics, IFAC Proceedings Volumes 39 (18) (2006) 171–176, doi:10.3182/20060920-3-fr-2912.00034.